Journal of Solid State Chemistry **147,** 281–290 (1999)
Article ID jssc.1999.8272, available online at http://www.idealibrary.com on IDEAL®

Nucleation and Growth of Icosahedral Boron Suboxide Clusters at High Pressure

Paul F. McMillan,*,†,[1] Hervé Hubert,† Andrew Chizmeshya,† William T. Petuskey,* Lawrence A. J. Garvie,‡ and Bertrand Devouard§

*Department of Chemistry and Biochemistry, Arizona State University, Tempe, Arizona 85287-1604; †Center for Solid State Science, Arizona State University, Tempe, Arizona 85287-1704; ‡Department of Geology, Arizona State University, Tempe, Arizona 85287-1804; and §Département de Géologie, UMR 6254 Magmas et Volcans, 5 rue Kessler, F-63038 Clermont-Ferrand, France

Received October 30, 1998; in revised form March 1, 1999; accepted March 11, 1999

The stoichiometry of boron suboxide ($B_6O_{1-\delta}$) synthesized from mixtures of boron and boron oxide (B_2O_3) at high pressure lies closer to the nominal composition ($\delta = 0$) than materials obtained at atmospheric pressure. The materials obtained in the high pressure syntheses in the presence of molten B_2O_3 also have a higher degree of crystallinity than for sintered powders. For syntheses at temperatures of 1700–1800°C at pressures between 4 and approximately 5.5 GPa, the well-crystallized particles are dominated by icosahedral multiply-twinned particles up to approximately 40 μm in diameter. This unusual morphology is obtained by Mackay packing, i.e., by assembly of successive shells of icosahedral B_{12} units around a central icosahedral nucleus to give a multiply twinned particle in which each of the 20 elements has the $R\bar{3}m$ space group of the rhombohedral α-B structure. We examine the thermodynamic and kinetic factors associated with the development of this morphology during high pressure growth and use *ab initio* calculations to investigate the energetic driving forces for initiation of the Mackay packing around the central icosahedral nucleus.

INTRODUCTION

Boron-rich solids form a class of light element-containing "super-hard" materials, with high tensile strength and large values of the bulk modulus and cohesive energy. The cubic phase of boron nitride (c-BN) is the second hardest known material (Vickers hardness H ~ 60 GPa), after diamond (H ~ 130 GPa for the 100 family of faces; ~ 170 GPa for {111}). The third hardest is boron suboxide (nominally B_6O), with an indentation microhardness reported at 38 GPa (1). This material has a crystal structure based on packing of B_{12} icosahedral units, derived from the metastable "α-rhombohedral" phase of boron (Fig. 1). The "icosahedral" boron-rich compounds have been the subject of intense study for over two decades, in part because of their desirable abrasive qualities and high resistance to wear: there have even been reports that samples of material with nominal composition near "$B_{22}O$" scratch the softer {100} faces of diamond (2). The icosahedral borides also pose both scientifically interesting and geometrically pleasing problems in solid state structural chemistry and in bonding theory. The electronic properties of these compounds, although still poorly understood, are known to be interesting and could be technologically useful (1–13).

There have been several previous reports of "B_6O" synthesized at or near ambient pressure, formed by reaction of elemental B with B_2O_3 or by oxidation of boron with zinc oxide or other oxidants (2–6). These syntheses typically produced fine-grained powders mixed with amorphous (a-B) material. Near-fully dense material has also been obtained by hot-pressing (2, 3, 7). When analyzed, these B_6O materials are generally nonstoichiometric with reported compositions ranging from $B_6O_{0.72}$ to $B_6O_{0.86}$ (3, 8–10). Although no single crystals have yet been available for structure refinement, the crystal structure has been well determined from powder data.

The α-boron structure (space group $R\bar{3}m$) consists of eight B_{12} icosahedra situated at the vertices of a rhombohedral unit cell and can be described as a distorted cubic close packing (ccp) of the icosahedral units (Fig. 1). In B_6O, two O atoms are located in the interstices along the [111] rhombohedral direction, replacing the 3-center, 2-electron bond that links the icosahedra in this direction in the α-B structure (6, 10).

We have recently reported synthesis of B_6O materials using high pressure–high temperature synthesis methods from mixtures of B and B_2O_3 (11–13). These syntheses yielded compounds with compositions close to the nominal one (i.e., with stoichiometry up to $B_6O_{0.96}$) and with much higher crystallinity than obtained for the room pressure syntheses. Large (up to 40 μm) euhedral grains were recovered in some runs.

[1] To whom correspondence and request for materials should be addressed.

0022-4596/99 $30.00

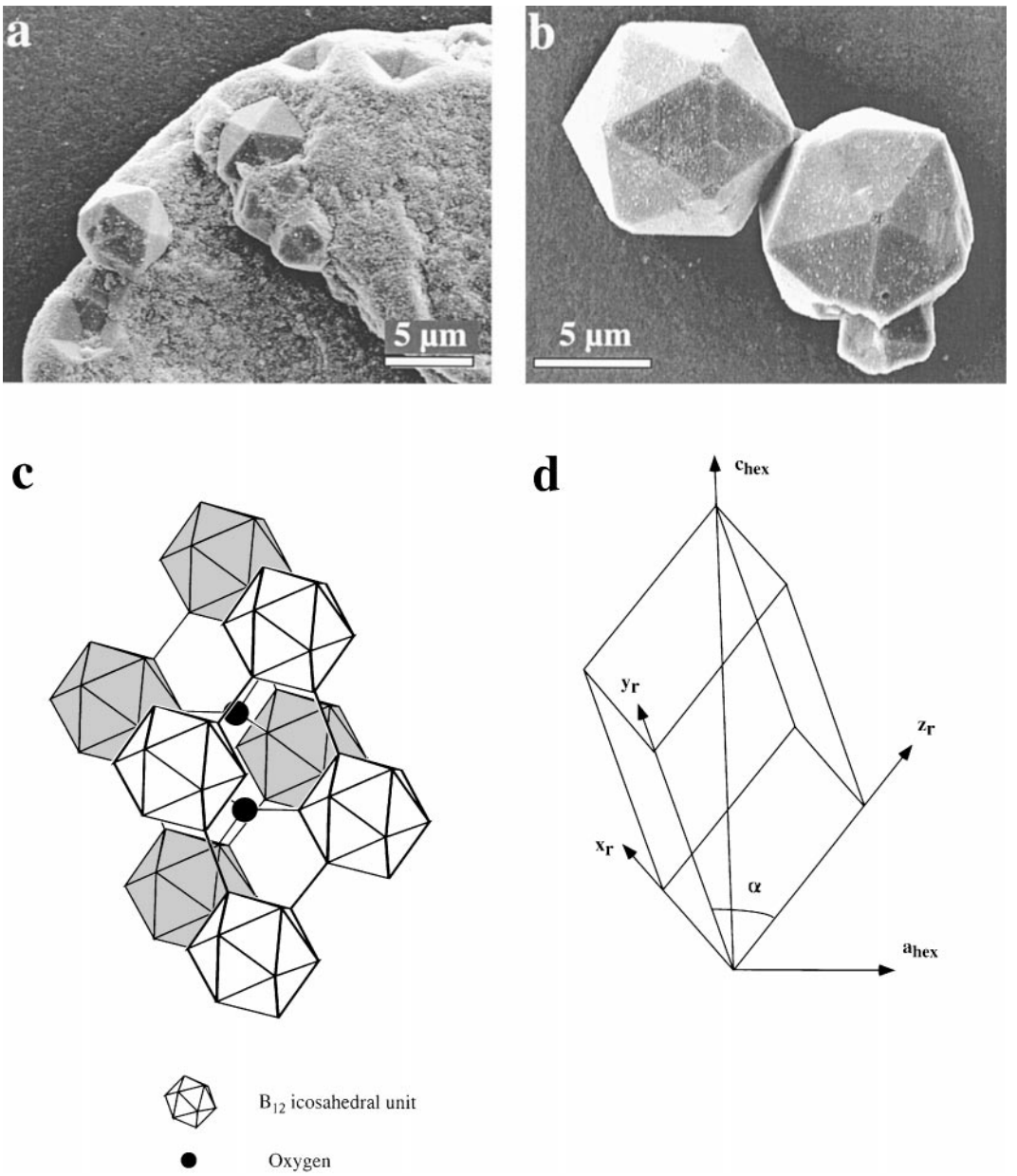

FIG. 1. (a) Scanning electron micrograph of B_6O icosahedral multiply-twinned particles (MTPs) in a fine-grained matrix derived from the B_2O_3–B_6O molten phase present in the high pressure synthesis experiments. (b) Two icosahedra free of matrix, one oriented along a 3-fold axis (triangular face) and the other along a 5-fold axis. The re-entrant features indicative of multiple twinning are visible at the apices (the surface appears flat because the depression created by re-entrant faces is filled with fine-grained material). (c) The structure of "ideal" (i.e., fully stoichiometric) B_6O with space group $R\bar{3}m$, derived from the α-rhombohedral structure of elemental boron with eight (slightly distorted) B_{12} icosahedra at the apices of the rhombohedral unit cell. Icosahedra shown in gray are in background. Oxygen atoms (dark) are three-coordinated to boron atoms in separate icosahedra. (d) An outline of the rhombohedral unit cell with rhombohedral (x_r, y_r, z_r) and hexagonal (c_{hex}, a_{hex}) axes shown. The base of the rhombohedron defines a tetrahedral figure in which the angle α may be distorted from the ideal tetrahedral value (70.5°), depending upon the ratio c_{hex}:a_{hex}. (see Refs. 12, 13.)

In addition, large (also up to 40 μm in diameter) near-perfect *icosahedral* particles were obtained in syntheses at 4–5.5 GPa (Fig. 1). This was an unusual and unexpected result, because the X-ray powder diffraction pattern remained fully consistent with the $R\bar{3}m$ space group, which does not allow the presence of five-fold symmetry. The presence of re-entrant faces on some particles allowed the identification of these icosahedra as multiply-twinned particles, rather than quasi-crystalline materials (12). We surmised that these particles had grown within the molten

B_2O_3 flux via "Mackay packing," in which successive shells of icosahedral B_{12} units formed around a central icosahedral nucleus (14). In the present study, we have undertaken a further investigation of the factors affecting the development of this unusual morphology under the high pressure synthesis conditions.

EXPERIMENTAL

The synthesis and characterization of B_6O at high pressures has been described in detail previously (11–13). Syntheses were carried out in a Walker-type multianvil apparatus from mixtures of amorphous B and B_2O_3 in various ratios. Samples were pressurized to between 1 and 10 GPa and then heated at 1200 to 1800°C from several minutes up to several hours. Phases present in the recovered sample were determined by X-ray diffraction and also by electron microscopy. Compositions were determined by parallel electron energy-loss spectroscopy (PEELS). Sample morphologies and atomic scale structure were examined with scanning electron microscopy, optical microscopy, and transmission electron microscopy (Figs. 1–3).

OBSERVATION OF ICOSAHEDRAL PARTICLES OF B_6O

From the analysis of run products synthesized at a range of pressures, temperatures, and starting compositions, the icosahedral particles only grew appreciably in the pressure range 4–5.5 GPa, at temperatures of 1700–1800°C, in the presence of a slight excess of B_2O_3 (11–13). For synthesis pressures below approximately 3 GPa, the oxygen content was always substantially below the nominal stoichiometry, in the range 0.73–0.85 (11, 13). For higher synthesis pressures, the particle compositions were found to be much closer to the stoichiometric value. It thus appears that increasing the synthesis pressure in the presence of an oxidizing agent results in an increase in the oxygen chemical potential, as should be expected, and that this drives the composition of the B_6O phase closer to the nominal stoichiometry. This process must play a key role in the formation of the icosahedral particles in the high pressure synthesis.

An additional key element in the development of our understanding of the problem was the observation, by high resolution transmission electron microscopy, of B_6O particles up to 50 nm in diameter present in the groundmass containing the macroscopic icosahedral particles. These nanometer scale particles consisted of multiply-twinned radiating assemblages with five-fold symmetry (12,13) (Fig. 2). We believe that these particles grew from individual B_{12} icosahedral units "decorated" with bound oxygen atoms present within a molten B_2O_3–B_6O phase and that they represent the initial stages of nucleation of the macroscopic icosahedra which formed via Mackay packing, described below.

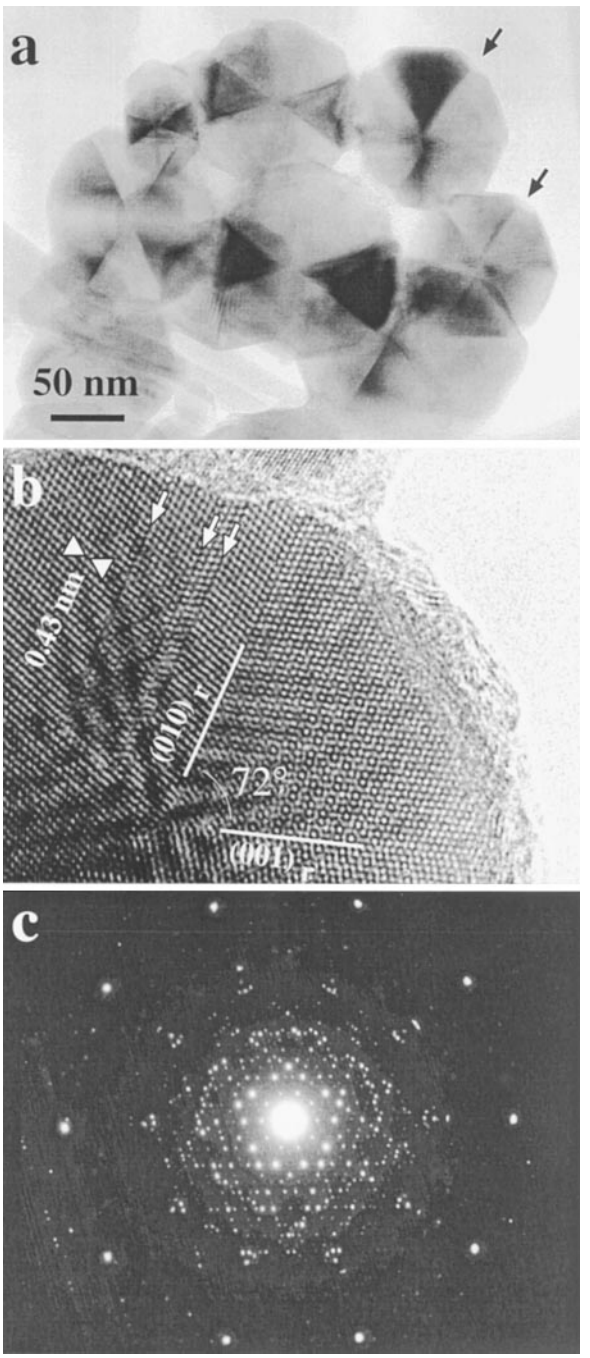

FIG. 2. (a) Low-magnification TEM image of B_6O MTPs showing individuals in Bragg orientation (darker). Re-entrant angles are arrowed. (b) High-resolution TEM image of a portion of a B_6O MTP in $[100]_r$ (rhombohedral setting) zone axis orientation, along the 5-fold axis of the icosahedron. Additional "stacking faults" (arrowed) are visible parallel to one of the twin planes. The moiré effect visible in the central part of the particle results from the superposition of the other twin individuals. (c) Selected-area electron diffraction pattern of a B_6O icosahedral MTP, showing the five-fold symmetry. Note the intense spots defining the inner pentagonal pattern at $1/0.436\ nm^{-1}$ ($1/d(100)r$) and $1/0.37\ nm^{-1}$ ($1/d(110)r$). (see Ref. 12.)

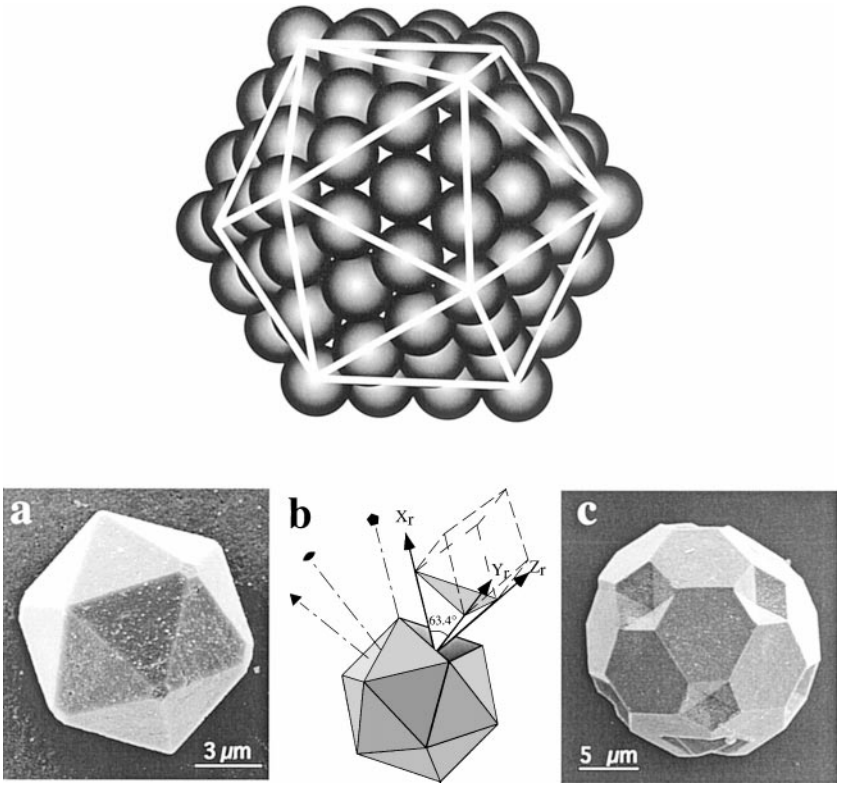

FIG. 3. (Top) An element of icosahedral (Mackay) sphere packing. The central sphere is surrounded by 12 others arranged at the corners of an icosahedron; successive layers are built up by placing additional spheres above the interstices in the layer below in a ccp arrangement. This propagates growth of the 20 triangular faces to give a macroscopic icosahedral figure. Mackay packing is space filling but does not possess translational symmetry and is less dense than conventional ccp because the separation between spheres in the plane of each triangular face is ~ 1.05 times their diameter (14). (Bottom) Morphology of B_6O MTPs. (a) Scanning electron microscopy (SEM) image of an isolated icosahedron. (b) Descriptive model of a regular icosahedron consisting of 20 tetrahedral individuals, illustrating the relationship between a tetrahedral individual and a rhombohedral cell. The rhombohedral unit cell of B_6O with $\alpha = 63.1^\circ$ matches the requirement for ideal icosahedral twinning ($\alpha = 63.4^\circ$). (c) SEM image of B_6O MTPs with well-developed faces forming e-entrant angles at the apices, indicative of twinning. This grain exhibits the same morphology as the C_{60} molecule. (see Ref. 12.)

MACKAY PACKING

In 1962, A. Mackay described a noncrystallographic packing scheme for identical spheres, which consisted of assembling succssive shells around a central icosahedron (14, 16). In the ccp arrangement of spheres, each coordination environment around a central sphere forms a cuboctahedral figure. As initially pointed out by R. Buckminster Fuller and developed by Mackay, the cuboctahedron can be easily distorted into an icosahedron. The radiating icosahedral "Mackay packing" scheme is then propagated by a cubic packing of spheres on each of the triangular faces (Fig. 3). However, this is *not* a closest packing arrangement: the spheres are separated by a distance equal to 1.05 times their diameter in the plane of the triangular face, so that the packing arrangement is less dense than ccp (14). Mackay concluded that "The possibility of the natural occurrence of icosahedral shell packing might be considered but there are several reasons which make it unlikely that large numbers of atoms might be found arranged in this way …" (14). There are several unique features of the B_6O structure, in which the B_{12} icosahedra play the role of the spheres being packed and the oxygen atoms act as "spacers" between the icosahedra in one family of planes, that permit Mackay's packing scheme to be realized under certain conditions.

The $R\bar{3}m$ structure of the α-rhombohedral borides can be described by either a hexagonal or a rhombohedral cell, derived from an axially distorted ccp arrangement of near-spherical B_{12} icosahedra (3,4,6,10,15) (Fig. 1). The rhombohedron is constructed from two tetrahedra capping a central octahedron. The c/a ratio of the underlying hexagonal cell indicates the degree of distortion of each tetrahedron. For example, the c/a ratio of near-stoichiometric B_6O at ambient pressure is $12.319{:}5.386 = 2.29$ (11–13, 15), giving an angle subtended at the apex of the tetrahedron of 63.1° (11–13). This is very close to the value (63.4°) required by the Mackay scheme for packing of twenty such distorted tetrahedra to obtain an icosahedrally twinned object (14)

(Fig. 3). The "magic" value of the c/a ratio required for such icosahedrally twinned particles is 2.26. These geometrical relationships are described in detail elsewhere (12,13,16).

Apart from B_6O, the only other rhombohedral borides to closely match this distortion index are $B_{12}Be$ (15) and "B_6N" (11,12). However, these materials have to date only been obtained by solid state sintering, not an environment favorable for development of large crystals or ideal morphologies. Boron suboxide prepared at or near ambient pressure consists of small (~ 1 μm) particles. In contrast, the available thermodynamic data, along with the texture of our recovered samples, indicate that the B_6O materials prepared in our studies at high pressure were obtained in the presence of a B_2O_3-rich molten phase, which would permit the growth of large crystals or particles. This is illustrated by consideration of a hypothetical schematic phase diagram for the B–O between B_2O_3 and B_6O systems at high pressures (Fig. 4).

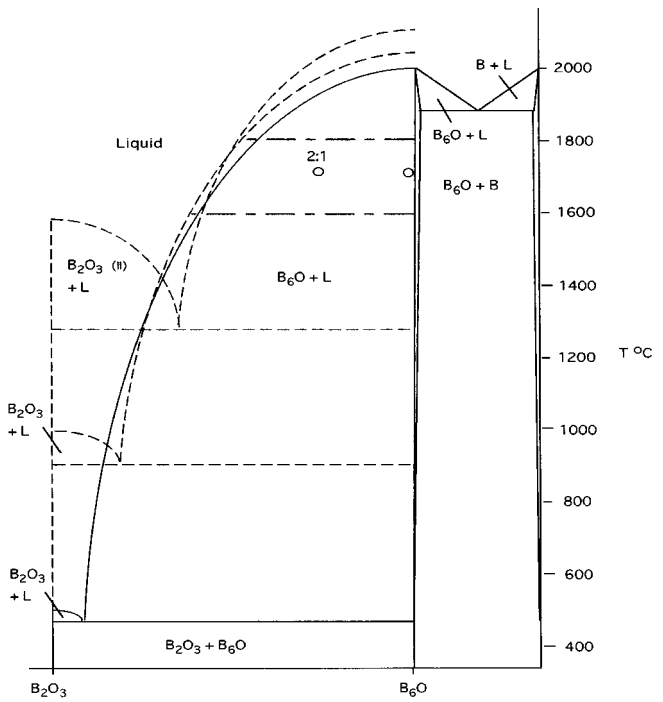

FIG. 4. A possible schematic phase diagram for the B_2O_3–B system, at low (< 1 GPa) pressure, moderate (~ 4–5 GPa) pressure, and high (~ 10 GPa) pressure, in the region of the presumed B_2O_3–B_6O eutectic. Constructed using available thermodynamic data (17) for B_2O_3 and B, and based on assumptions described in the text. B_2O_3 melting at high pressure (above the I–II transition) is extrapolated from (18). We have drawn considerable curvature to the melting slopes along the B_6O–B_2O_3 join to reflect likely nonideal mixing of liquid components (unmixing may even occur). The melting curve of B_2O_3 moves upward rapidly with P due to the crystalline B_2O_3 I–II transition at ~ 2–3 GPa. Melting relations of B and B_6O are expected to shift less with pressure, because crystals and liquid are expected to have similar volumes and compressibilities. Our experimental runs were conducted at 1600–1800°C, in the $B_6O + L$ field; points indicate the usual range of starting compositions.

A HYPOTHETICAL B–O PHASE DIAGRAM

There is little information available with which to construct a proper set of phase relations for B_6O, B_2O_3, and B at high pressure and high temperature that would be relevant to the present study. We have thus relied on our experimental observations (11–13) along with available thermodynamic data to propose a possible phase diagram for the B–O system that helps us understand the results of our experimental runs. A series of such diagrams is illustrated schematically in Fig. 4, for low (< 1 GPa), intermediate (~ 5 GPa), and high (~ 10 GPa) pressure.

First, we have ignored any thermodynamic difference between the metastable (α) and stable (β) rhombohedral phases of boron. These have quite different structures, but we assume that their melting relations are the same. At ambient pressure, β-boron melts at 2075°C (17). We expect the molar volumes of crystalline and amorphous boron phases based on boron–boron bonding to be of comparable magnitudes and the compressibilities to be small, so that the melting point should vary little with pressure. The boron suboxide phase is unstable above 1760°C at ambient pressure, breaking down to boron and gaseous B_2O_2 (3). For this reason, we draw the "low pressure" hypothetical phase diagram at a finite confining pressure, sufficient to stabilize the B_6O phase. The melting point of B_6O has not yet been determined at any pressure: however, we assume that it is similar to that of isostructural B_4C (17), and that the melting point is essentially indistinguishable from that of pure boron. We have presumed simple binary eutectic melting relations between B and B_6O. Prior experiments indicate that there is some small solubility of O in B (2) and there is some composition range of $B_6O_{1-\delta}$, at both low and high pressure; however, our results indicate that the B_6O phase in equilibrium with the B_2O_3-rich (liquid) component is nearly stoichiometric ($\delta \approx 0$).

At ambient pressure, the low pressure form of boron oxide (B_2O_3-I) has a very low melting temperature (~ 430°C) compared with that of the refractory borides (17), but this value increases with pressure to reach approximately 1100°C at 6 GPa (18). Above 2–3 GPa (depending upon the synthesis temperature), B_2O_3 transforms to an orthorhombic high pressure phase B_2O_3-II (18). Based on the results of the synthesis experiments of Mackenzie and Claussen (18), the melting slope of B_2O_3-II is likely to be steeper than that of the low pressure phase. We have carried out a "courageous" extrapolation from the phase relations sketched by these authors, and we estimate that the melting point of B_2O_3-II could reach a value on the order of 1600°C at 10 GPa. We recognize that this estimate of melting point for the B_2O_3 component could be seriously in error (most likely overestimated). We have carried out a series of molecular dynamics calculations (J. Diefenbacher, unpublished) that indicate that the B_2O_3 liquid contains a mixture

of III- and IV-coordinated borate units at low pressure and that the average boron coordination in the liquid increases with increasing pressure, so that the melting temperatures of both crystalline phases could change in a non linear fashion and may even have a negative dT_m/dP slope, with increasing pressure (18). However, for the purposes of the present discussion, we expect that the melting point of the B_2O_3 component increases more rapidly than that of B_6O with increasing pressure.

We have no good constraints on the form of the melting relations between B_2O_3 and B_6O. We know from structural studies on glasses and liquids that pure B_2O_3 melts to a liquid cotaining essentially borate polymer units linked by "ionic" B–O bonds (18), whereas more "covalent" units with B–B bonding must dominate the liquids near the B and B_6O compositions. We expect that there is little driving force for formation of B–B linkages near the B_2O_3 composition, and thus we expect that the liquidus drops rather steeply from B_2O_3, perhaps to a eutectic close to B_2O_3. We have drawn considerable curvature to the melting slopes along the B_6O–B_2O_3 join to reflect the likely nonideality of mixing in the components: there might even be unmixing in the liquid state. We believe that the liquid in equilibrium with B_6O lies far toward the B_2O_3 composition.

In our experimental runs at high pressure, the samples were never completely molten (13), consistent with our schematic phase diagram (Fig. 4). Examination of the groundmass (Fig. 1) recovered from our high pressure experiments shows small (up to 50–100 nm across) icosahedral particles (Fig. 2) contained within an "ionic" borate matrix (this material was either easily hydrated and removed in low pressure runs or recrystallized as nanoscale B_2O_3-II when quenched from higher pressures); this groundmass or matrix likely represents the quenched liquid phase present in the synthesis experiments, in equilibrium with the growing B_6O crystalline particles. We propose that "B_{12}" icosahedral clusters dissolved within the ionic-covalent B_6O–B_2O_3 liquid phase in equilibrium with crystalline B_6O could have provided nuclei for the growth of Mackay polyhedra of the crystalline B_6O.

Most of our experimental synthesis runs were conducted at 1600–1800°C, with starting B_2O_3:16B ratios extending up to 2:1. From the schematic (hypothetical) phase diagram, these compositions would give rise to crystalline B_6O in equilibrium with a liquid phase close to B_2O_3 in composition, consistent with our experimental observation of growth of large particles in a quenched nanocrystalline, partly amorphous groundmass. One series of runs at 10 GPa was carried out at 1200°C, and these gave rise to only sintered fine grains of crystalline B_2O_3 and B_6O (13): such runs were obviously subsolidus.

These results illustrate the importance of the presence of a liquid phase in the growth of large grains, including the macroscopic icosahedra. However, at pressures below 4 GPa, no large particles were observed to grow, despite the presence of liquid. The B_6O particles obtained were < 1 μm in size and were generally found to be nonstoichiometric (11). Above this pressure, large icosahedral particles with close to ideal stoichiometry were found to be present, and these were easily separated from the fine grained groundmass (Fig. 1). It is obvious that some factor other than the presence of the borate liquid flux operates to cause the nucleation and growth of the macroscopic B_6O icosahedral particles at pressures above 3–4 GPa. This factor is likely to include the oxygen content of the phase.

From a macroscopic point of view, successful completion of the Mackay packing scheme requires that the 20 tetrahedral twins that constitute the multiply-twinned icosahedral particle be distorted such that the apical angle α that constitutes the angle between the basis vectors of the rhombohedral cell lies close to 63.4° (Fig. 3) or that the c/a ratio of the alternative hexagonal cell lies close to the "magic" value of 2.26. It is known that the c/a ratio of $B_6O_{1-\delta}$ decreases with increasing oxygen content, from 2.295 for a sample of $B_6O_{0.76}$ prepared in our studies at ambient pressure to 2.284 for $B_6O_{0.96}$ obtained at 5.5 GPa (13); i.e., in a macroscopic sense, the increasing oxygen content of the B_6O phase at higher pressure brings the c/a ratio closer to the value required for successful Mackay packing. Further, we now have preliminary data that indicate that the c/a ratio decreases further at high pressure, during *in situ* compression (G. Wolf and K. Leinenweber, unpublished). We propose then that increasing the synthesis pressure increases the chemical potential of oxygen and hence the oxygen content of the B_6O phase, reducing its c/a ratio, until above 3–4 GPa the required distortion index of the rhombohedral structure is achieved for Mackay packing to be realized in macroscopic form.

We now turn to an exploration of the microscopic nature and energetics of this process by a series of *ab initio* and semi-empirical cluster calculations designed to explore the relative stability of various oxygenated clusters and to investigate the initial stages of formation of the icosahedrally twinned particles by agglomeration of oxygen atoms and additional B_{12} icosahedra about a central B_{12} icosahedral unit dissolved in the B_2O_3 melt.

THEORETICAL STUDY

Two series of cluster calculations were carried out to investigate the initial stages of oxidation of (a) icosahedral B_{12} units (the "bare" cluster) and (b) the supericosahedral $B_{12}(B_{12})_{12}$ cluster (Fig. 5). Accurate all-electron Kohn–Sham (AEKS) density functional theory (DFT) calculations were first carried out for the primitive icosahedral (B_{12}) units using the LCGTO (linear combination of Gaussian-type orbitals) molecular code DeFT (19). The formal electron counting scheme for boron icosahedra assigns two

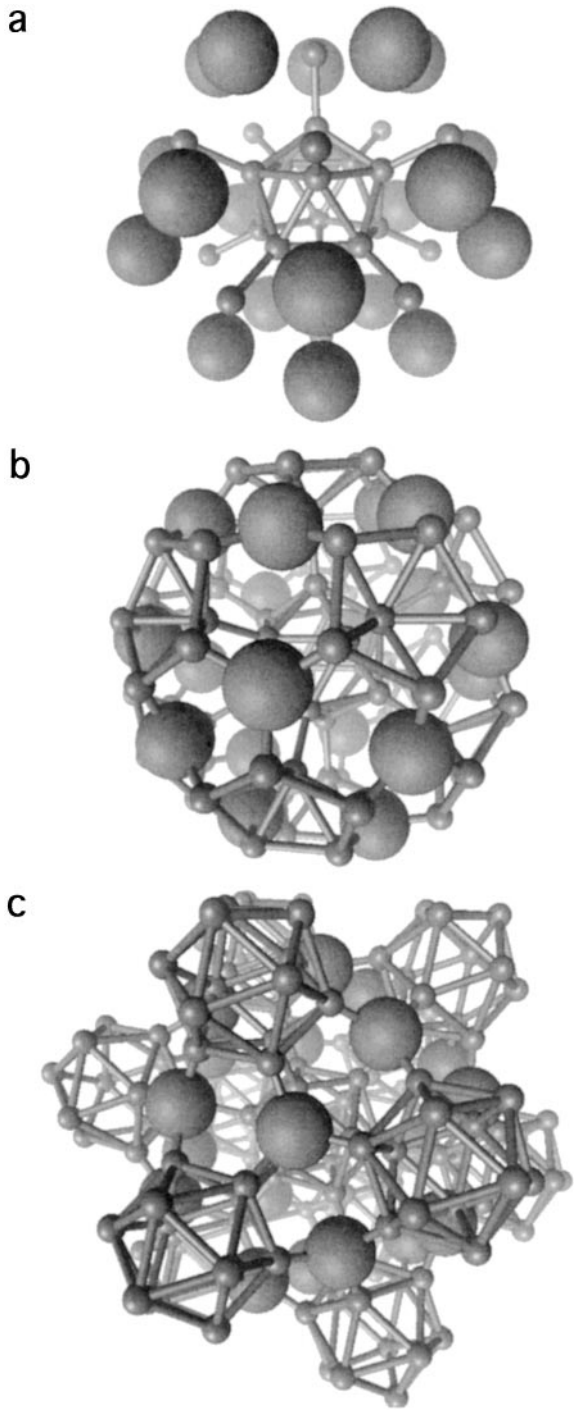

FIG. 5. Progression of structural modifications illustrating the supericosahedral structure described in our energetics calculations. (a) The central boron icosahedron surrounded by 12 intericosahedral boron atoms (not included in the "bare cage" calculations) and the 20 oxygens denoted by red spheres. The latter sit above the icosahedral faces of the central icosahedron. For "bare cage" calculations, oxygen atoms were sequentially added to the central B_{12} icosahedron. (b) As for (a), but with the next near neighbor shell of borons from the adjoining icosahedral cages included. Oxygen–boron bonds are clearly seen from this hypothetical perspective. (c) The completed supericosahedral cage consisting of 13 B_{12} cages and 20 oxygen atoms ($B_{156}O_{20}$). Calculations were carried out for clusters with oxygen atoms added sequentially to the supericosahedron.

electrons to a "core" state internal to the icosahedron and with equal participation from all 12 B atoms, 24 electrons distrbuted among 12 two-electron three-centered "shell" states on the surface of the icosahedron, and an additional 12 electrons in "dangling bond" states available for bonding exterior to the icosahedron. Complete filling of all these states requires a total of 38 electrons (20). The neutral, isolated ("bare") B_{12} icosahedron is formally electron deficient (36 valence electrons) and might be expected to show some structural or electronic instability. This was revealed in the results of the AEKS calculations, which showed that the B_{12} icosahedron is structurally unstable with respect to "flattening" of the icosahedral unit. The addition of two electrons (to form the B_{12}^{2-} ion) removed the structural instability. We conclude that charge compensation or covalent linkage to other structural units is required to avoid structural collapse of the icosahedral unit, as is observed experimentally (20). This requirement for added bonding would provide a driving force for bonding to oxygen atoms or to other icosahedra present in the B_2O_3–B_6O melt in our synthesis experiments. We have examined the energetics of oxidation of both icosahedral B_{12} and supericosahedral $B_{12}(B_{12})_{12}$ cluster units in our calculations (Fig. 5).

The accurate AEKS calculations could not be extended to larger clusters. Instead, clusters containing as many as 600 electrons were treated using the self-consistent field (SCF) semi-empirical AM1 model (21) and in calculations using a local-orbital ("Fireball") Harris basis (22). Consistent with both the empirical electron counting scheme and the *ab initio* AEKS calculation results, the AM1 and "Fireball" calculations yielded a molecular orbital eigenvalue spectrum for the basic B_{12} unit consisting of a low lying doubly occupied A_g core state, and a manifold of "shell" and dangling bond states deriving from the *s*–*p* boron valence states. The HOMO state is either three-fold degenerate and partially occupied (local orbital Harris) or doubly occupied and nearly degenerate with two other two-electron states, one of which remains unfilled (AM,1 and AEKS) (Fig. 6).

We studied the initial growth morphology of icosahedral B_6O particles by investigating the oxidation energetics of B_{12} and the supericoshedral $B_{12}(B_{12})_{12}$ cluster, mainly using the AM1 model (24). The results indicate that the electron deficient B_{12} unit is stabilized either by addition of one to two oxygens to the icosahedron or by binding to another icosahedron (Fig. 7). Further addition of oxygen atoms serves to destabilize the oxygenated cluster, however, in these calculations at zero pressure and temperature. We can already conclude at this stage, however, that a "free" icosahedral unit B_{12} in the melt would quickly attach itself to another icosahedron, or to oxygen, thus initiating the growth of supericosahedral units.

We then investigated the formation of a supericosahedral cluster by arranging tweleve B_{12} units around a central B_{12}

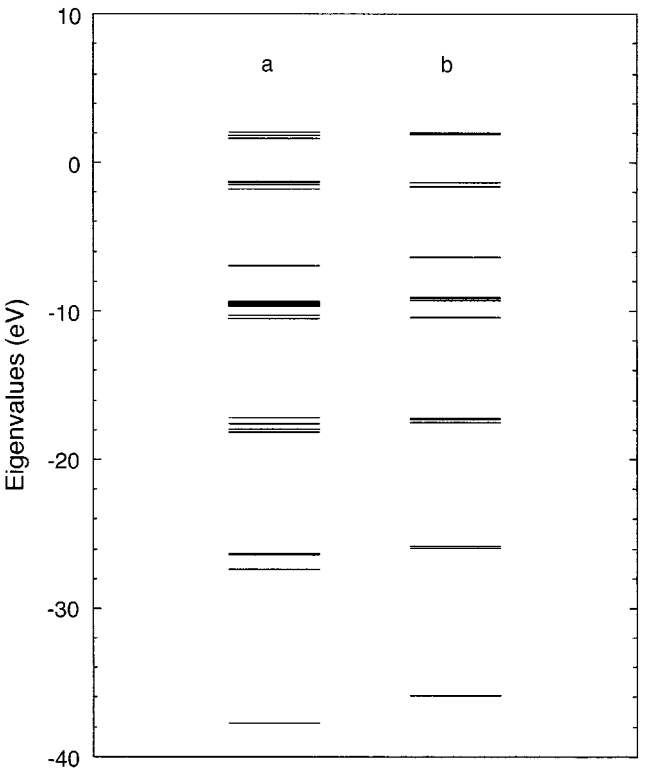

FIG. 6. Molecular orbital eigenvalue diagrams for the icosahedral B_{12} unit from (a) AM1 and (b) local orbital "fireball" calculations, choosing I_h symmetry and a B–B bond equal to the average in the crystal. The energy levels in both cases correspond to (i) a low lying doubly occupied A_g icosahedral "core" state, and (ii) a manifold of "shell" and "dangling bond" states deriving from the *s*–*p* boron valence states. The HOMO state is either three-fold degenerate and partially occupied (local orbital) or doubly occupied and nearly degenerate with two other two-electron states, one of which remains unfilled (AM1 model).

molecule (Fig. 5). For charge compensated B_{12}^{2-} molecules the AM1 model predicts a B–B bond length of 1.81 Å, in good agreement with the experiment (average 1.83 Å for the crystalline phase). A value of 1.64 A was used for the intericosahedral B–B bond length. The 20 sites were centered above the 20 corresponding faces of the central icosahedron. These oxygens (not bonded to the central icosahedron) form three equal bonds of length 1.43 A to first icosahedral shell borons, as found in crystalline B_6O.

The oxidation energetics were studied by computing the reaction energy per oxygen atom as a function of oxygen number. The energy of the bare $13(B_{12})$ cluster is subtracted from the oxidated cluster energy and divided by the number of oxygen atoms abosrbed. Subtracting a neutral oxygen energy from this quantity then gives the net reaction energy per oxygen as a function of oxygen site occupation. This quantity is plotted in Fig. 7, where it can be seen that the energy gain is largest at the onset of oxidation (-11.85 eV). However, adding additional oxygens up to the maximum value of 20 (filling all the available sites on the surface of the supericosahedron) is an endothermic process, requiring ($-10.33- -11.85 = 1.52$ eV per oxygen atom added). Also shown in the figure is the result of similar calculation for a single B_{12} unit. Again, the largest energy gain is observed at the onset of oxidation, but the value (8.5 eV) is somewhat smaller than for the $13(B_{12})$ cluster indicating that the attachment of additional boron icosahedra significantly enhances the oxidation process. As a calibration point, a high-quality all-electron calculation (FP LAPW [23]) in the $R\bar{3}m$ crystalline phase (i.e., α-B vs B_6O) yielded an oxidation reaction energy per oxygen atom of 9.8 eV (25).

These results indicate that adding additional oxygens to the supericosahedral cluster is an endothermic process. However, in order to propagate the Mackay packing, all of the 20 oxygen sites on the surface of the supericosahedron must be filled, otherwise the B_{12} icosahedra would not be held sufficiently "apart" (i.e., by 1.05 *D*, where *D* is the icosahedral diameter) for successful "space filling" in Mackay's sense on the surface of the growing icosahedrally twinned particle (compare Figs. 3, 4, and 5). Hence, additional energy must be provided in the form of a chemical potential driving force to fully oxygenate the supericosahedral cluster, in order for the Mackay packing to propagate. We believe that this is the role played by the high pressure variable in the experimental study. The oxygen chemical potential developed above 4 GPa in the oxidation reaction could

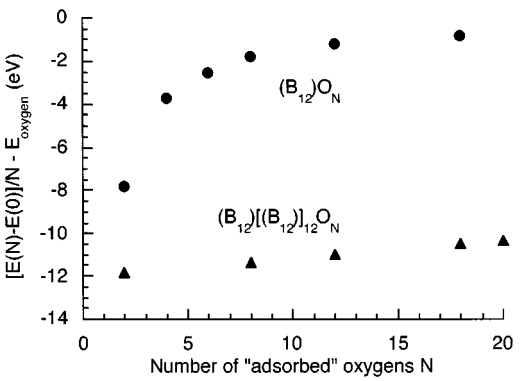

FIG. 7. Energetics of oxidation of icosahedral (B_{12}) and supericosahedral ($B_{12}(B_{12})_{12}$) clusters, using the semi-empirical AM1 model (21). The supericosahedral cluster was formed by arranging 12 B_{12} units around a central B_{12} molecule, using 1.64 A for the intericosahedral B–B bond length. The 20 available oxygen sites were centered above the 20 corresponding faces of the central icosahedron. These oxygens (not bonded to the central icosahedron) form three equal bonds of length 1.43 A to first icosahedral shell borons, as found in crystalline B_6O. Oxidation energetics were computed as the reaction energy per oxygen atom as a function of oxygen number (*N*). The energy of the bare $13(B_{12})$ cluster is subtracted from the oxide-rich cluster energy and dividided by the number of oxygen atoms absorbed. Subtracting a neutral oxygen energy from this quantity then gives the net reaction energy per oxygen as a function of oxygen site occupation. Also shown in the figure is a similar calculation for a single B_{12} unit. Again, the largest energy gain is observed at the onset of oxidation, but the value (8.5 eV) is somewhat smaller than for the $13(B_{12})$ cluster.

easily be on the order of tens or even hundreds of kJ/mol. This point is discussed in the next section, where we return to thermodynamic arguments.

THERMODYNAMIC ANALYSIS

The oxidation reaction to form $B_{12}O_2$ (i.e., one formula unit of B_6O) can be written as

$$B_{12}\square_2 + O_2 \rightarrow B_{12}O_2, \qquad [1]$$

where the "$B_{12}\square_2$" is defined as an oxygen-free α-boron structure, with the same ("stretched") volume as B_6O at P and T. We have carried out accurate *ab initio* calculations using the FP LAPW (23) for the crystalline solid reference states α-B_{12} and "$B_{12}\square_2$," and have determined that the internal energy of the stretched state lies 61.82 kJ/unit cell above that of the α-B_{12} phase at room pressure. A further calculation indicated that the $B_{12}O_2$ phase lies 1306.3 kJ/unit cell below the $B_{12}\square_2$ standard state. We then construct a mixing relation between $B_{12}O_2$ and $B_{12}\square_2$ of the form.

$$\begin{aligned}\Delta G_f(s.s.) = [&-1{,}244{,}500 + 1{,}306{,}300x] \\ &- T\{-200(1-x) - 2R[x\ln x \\ &+ (1-x)\ln(1-x)]\} + \Delta g^{excess}_{mixing}, \end{aligned} \qquad [2]$$

where x is the mole fraction $B_{12}O_2$. The term in $\Delta g^{excess}_{mixing}$ includes $\Delta h^{excess}_{mixing}$ of O and holes ("$\square$"), in the "expanded" α-B_{12} structure, and $\Delta s^{excess}_{mixing}$ which includes nonconfigurational effects such as vibrational terms. Both of these terms could be substantial, especially at the high run temperatures; however, we must ignore them here for lack of data. From existing thermodynamic data (JANAF tables), we estimate ΔG for the formation reaction α-$B_{12} + O_2 \rightarrow B_{12}O_2$ to be $(-1{,}244.5 + 200T)$ kJ/unit cell, where T is the absolute temperature. As a first approximation, we assume that mixing of O and $\square$ in the expanded α-B_{12} structure is ideal. The free energy change upon melting of β-boron is 89.232 kJ/unit cell (ΔG for a B_{12} unit: JANAF tables), so that the B_{12} liquid phase lies 24.408 kJ/unit cell above the "expanded" α-$B_{12}\square_2$ structure. By taking into account the cohesive energy O_2 molecules relative to O atoms, the energy difference between $B_{12}O_2$ and $B_{12}\square_2$ at low temperature is 1,244.5 kJ/unit cell. These relations permit us to establish the basis for the free energy diagram shown in Fig. 8.

This figure illustrates schematically the dependence of the Gibbs energy of formation on composition and phase that is consistent with the proposed phase diagram (Fig. 4). It corresponds to an arbitrary temperature between the melting points of B_6O and B_2O_3. As described above, we depict $B_6O_{1-\delta}$ as a solid solution between stoichiometric

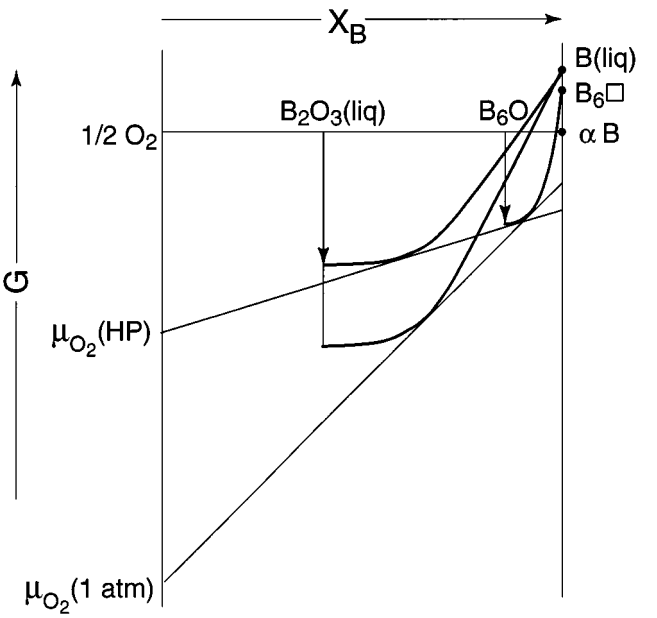

FIG. 8. Schematics of the Gibbs energies of the $B_6(O, \square)$, in the "expanded" α-B_{12} structure, and $\Delta s^{excess}_{mixing}$ (which includes nonconfigurational effects) solid solution and the B_2O_3–B_{12} liquid solution at both low and high pressures to illustrate the relative shift in oxygen: boron stoichiometry in the crystalline $B_6O_{1-\delta}$ phase. Increasing pressure results in an increase in the chemical potential of oxygen in the system (μ_{O_2}). This occurs mainly because the molar volume of the B_2O_3-rich liquid phase is greater than that of the icosahedral boron-rich phases. The result is an increase in oxygen content (i.e., decreasing δ) in the crystalline $B_6O_{1-\delta}$ phase (i.e., the common tangent at high pressure moves toward the nominal B_6O stoichiometry). The "1 atm" $G(X)$ curves correspond to an arbitrary temperature between the melting points of B_2O_3 and B_6O at low pressure (sufficiently above 1 atm to stabilize B_6O). The Gibbs energies for the solutions at "high pressures" are overlayed onto these schematic curves at low pressure.

B_6O and an isotropically "stretched" form of α-B, i.e., $B_6\square$, where $\square$ represents an oxygen vacancy. We assume that the solid solution can be described as the ideal mixing of oxygen and vacancies on the three-fold coordination sites that link the boron icosahedra. As such, the enthalpy of mixing is assumed to be zero.

The liquid solution is likely to consist of a mixture of fundamental structural units with B–O and B–B bonding. At one compositional extreme, B_2O_3 consists of three- and four-fold oxygen-coordinated boron, the latter of which is increasingly favored at higher pressures. We have no information on the solution thermodynamics; however, the downward, positive curvature of the Gibbs energy sketched in Fig. 8 corresponds to configurational entropy of mixing combined with probable contributions of excess entropy.

At low pressures, a two-phase equilibrium between solid $B_6(O, V)$ and the liquid solution would correspond to the lower common tangent indicated in Fig. 8. The composition of $B_6O_{1-\delta}$ would correspondingly be oxygen poor as would

the liquid solution. However, higher pressures differently affect the relative energies of the endpoints of the solid and liquid solutions. In the reaction

$$B_2O_3(l) + 16B(s) \rightarrow 3B_6O, \qquad [3]$$

the fractional volume change, $\Delta V/V_0$, is likely to be negative. Higher pressure, therefore, results in a more negative Gibbs energy change for this reaction, since $\Delta G_R \alpha \int \Delta V_R dP$. The "high pressure" relations in Fig. 8 illustrate this relationship as a relatively large increase in the Gibbs energy of liquid B_2O_3 and the curve associated with the liquid solution, compared with that of the $B_6O_{1-\delta}$ crystalline phase. The result is an increase in the oxygen contents of both $B_6O_{1-\delta}$ and the liquid, indicated by the new common tangent. Simultaneously, the oxygen chemical potential, indicated by the intersection of the common tangent with the $X_B = 0$ (pure O_2 component) axis increases at high pressure. The curves in Fig. 8 are constrained by the results of *ab initio* calculations on the solid materials, by thermodynamic data available for pure B_2O_3 liquid, and by the experimental determinations of compositions of $B_6O_{1-\delta}$ materials prepared at different pressures (11,13). From these constraints, we estimate an increase in μ_{O^2} on the order of 150 kJ/mole (g atom O), for a synthesis pressure of approximately 5 GPa. This value corresponds to the energy required to force full oxygenation of the $B_{12}(B_{12})_{12}$ clusters as discussed in the previous section, which in turn is required for growth of the macroscopic icosahedral units via Mackay packing.

CONCLUSIONS

The high oxygen activity developed in the experimental run charge in the high pressure synthesis experiment causes supericosahedral ($B(B_{12})_{12}$) clusters present within the boron oxide melt phase (or at the interface between the reactants solid boron and B_2O_3 liquid) to become fully oxygenated. This in turn satisfies the "distortion index" requirement for successive icosahedral shells to grow via Mackay packing. The presence of oxygen atoms in threefold planar coordination to boron holds the icosahedra apart from each other (by a distance equal to 1.09 times their diameter *D*), which is sufficiently close to the ideal value (1.05 *D*) found by Mackay for perfect simultaneous tiling of all of the triangular faces of an icosahedron by spheres of diameter *D* in his icosahedral packing scheme. At lower pressure, the oxygen activity is not sufficiently high, the degree of oxidation of icosahedral "nuclei" is not sufficiently complete to realize this requirement, and the multiply-twinned icosahedral particles cannot grow. At the present time, we have no good explanation for our observation that icosahedral particles no longer appear to grow above approximately 7.5 GPa. However, it is possible that the lower packing efficiency of the Mackay scheme compared with "normal" ccp (0.6882 for icosahedral packing compared with 0.7405 for ccp (14) comes into play at higher pressures.

ACKNOWLEDGMENTS

We dedicate this paper to the memory of Jean Rouxel. One of the co-authors (HH) knew him as an undergraduate student in Nantes: PFM spent a sabbatical leave in his group at the newly-founded Institut de Matériaux de Nantes. Jean enjoyed the combination of "practical" materials with beatutiful solid state structures; he also practiced the interplay between synthesis and characterization experiments to understand their formation and properties. Although neither a high pressure nor a boride chemist, Jean saw the present work in its early stages and shared our initial pleasure and wonder at the icosahedral particles. We also express our deepest appreciation to our colleague Mike O'Keeffe, who guided us to the work of A. Mackay, and who worked out the geometrical relationships for the icosahedral twins, published in our earlier work together. This work was supported by an ASU MRSEC award from NSF DMR-9632635.

REFERENCES

1. H. F. Rizzo, W. C. Simmons, and H. O. Bielstein, *J. Electrochem. Soc.* **109,** 1079 1962).
2. A. R. Badzian, *Appl. Phys. Lett.* **53,** 2495 (1988).
3. D. R. Petrak, R. Ruh, and B. F. Goosey, *in* "Proceedings of the 5th Materials Research Symposium," NBS Spec. Pub. 364, p. 605, 1972.
4. I. Higashi, M. Kobayashi, J. Bernhard, C. Brodhag, and F. Thévenot, *in* "Boron-Rich Solids," Vol. 231, p. 201. A.I.P Conference and Proceedings, 1991.
5. H. Bolmgren, T. Lundström, and S. Okada, *in* "Boron-Rich Solids," Vol. 231, p. 197. A.I.P Conference and Proceedings, 1991.
6. M. Kobayashi, I. Higashi, C. Brodhag, and F. Thévenot, *J. Mater. Sci.* **28,** 2129 (1993).
7. C. Brodhag and F. Thévenot, *J. Less-Common Metals* **117,** 1 (1986).
8. S. LaPlaca and B. Post, *Planseeber. Pulvermet.* **9,** 109 (1961).
9. R. A. Pasternak, *Acta Crystallogr.* **12,** 612 (1959).
10. T. Lundström and Y. G. Andreev, *Mater. Sci. Eng. A* **209,** 16 (1996).
11. L. A. J. Garvie, H. Hubert, P. R. Buseck, W. T. Petuskey, and P. F. McMillan, *J. Solid State Chem.* **133,** 356 (1997).
12. H. Hubert, L. A. J. Garvie, B. Devouard, M. O'Keeffe, P. R. Buseck, W. T. Petuskey, and P. F. McMillan, *Nature* **391,** 376 (1998).
13. H. Hubert, L. A. J. Garvie, B. Devouard, M. O'Keeffe, P. R. Buseck, W. T. Petuskey, and P. F. McMillan, *Chem. Mater.* **10,** 1530 (1998).
14. A. L. Mackay, *Acta Crystallogr.* **15,** 916 (1962).
15. T. Lundström, *in* "Boron-Rich Solids," Vol. 231, p. 186. A.I.P Conference and Proceedings, 1991.
16. M. O'Keeffe and B. G. Hyde, "Crystal Structures. I. Patterns and Symmetry." Mineralogical Society of America, 1996.
17. R. A. Robie, B. S. Hemingway and J. R. Fisher, *Geol. Survey Bull.* 1452 (1979).
18. J. D. Mackenzie and W. F. Claussen, *J. Am. Ceram. Soc.* **44,** 79 (1961).
19. D. St Amant, "DeFT: An All-electron LCGTO Density Functional Program," Dept. of Chemistry, University of Ottawa, Ontario Canada, 1996.
20. R. B. King, *Inorg. Chim. Acta* **198–200,** 841 (1992).
21. M. W. Schmidt, K. K. Baldridge, J. A. Boatz, J. H. Jensen, S. Koseki, M. S. Gordon, K. A. Nguyen, T. L. Windus, and S. T. Elbert, *QCPE Bulletin*, **10,** 52 (1990); *J. Comput. Chem.* **14,** 1347 (1993).
22. O. F. Sankey and D. J. Niklewski, *Phys. Rev. B* **40,** 3979 (1989).
23. P. Blaha, K. Schwarz, P. Dufek, and R. Augustyn, *WIEN95*, Technical University of Vienna, 1995. [Improved and updated Unix version of the original copyrighted WIEN-code: P. Blaha, K. Schwarz, P. Sorantin, and S. B. Trickey, *Comput. Phys. Commun.* **59,** 399 1990]